Accepted Manuscript

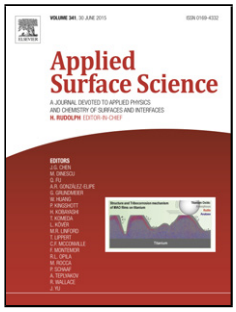

Title: DFT study of β-D-glucose adsorption on single-walled carbon nanotubes decorated with platinum. A bonding analysis

Authors: Alejandro J. González Fá, Valeria Orazi, Estela A. González, Alfredo Juan, Ignacio López-Corral

PII: S0169-4332(17)31582-9
DOI: http://dx.doi.org/doi:10.1016/j.apsusc.2017.05.227
Reference: APSUSC 36162

To appear in: *APSUSC*

Received date: 27-4-2017
Revised date: 20-5-2017
Accepted date: 25-5-2017

Please cite this article as: Alejandro J.González Fá, Valeria Orazi, Estela A.González, Alfredo Juan, Ignacio López-Corral, DFT study of β-D-glucose adsorption on single-walled carbon nanotubes decorated with platinum.A bonding analysis, Applied Surface Sciencehttp://dx.doi.org/10.1016/j.apsusc.2017.05.227

This is a PDF file of an unedited manuscript that has been accepted for publication. As a service to our customers we are providing this early version of the manuscript. The manuscript will undergo copyediting, typesetting, and review of the resulting proof before it is published in its final form. Please note that during the production process errors may be discovered which could affect the content, and all legal disclaimers that apply to the journal pertain.

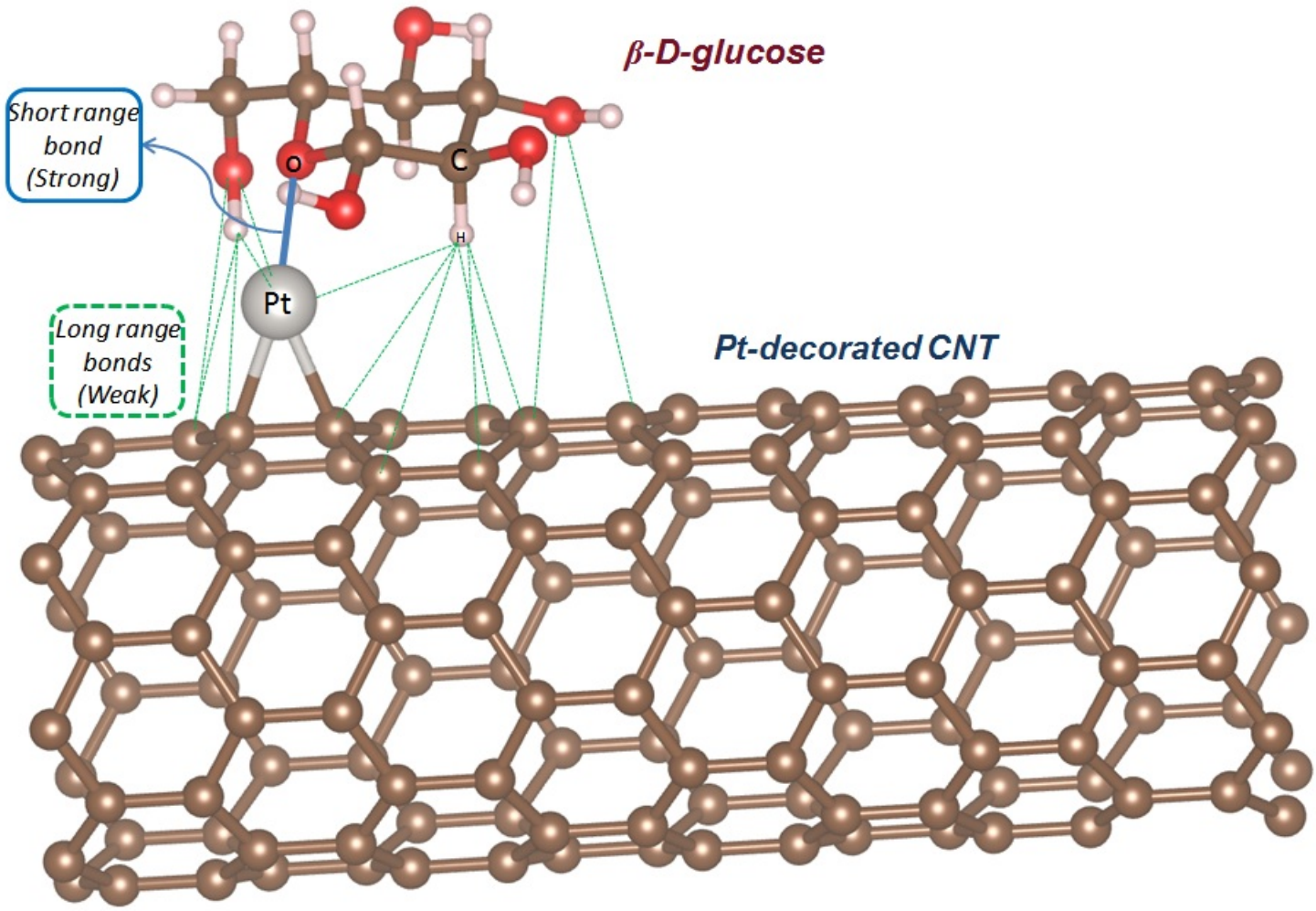
β-D-glucose
Short range bond (Strong)
O
C
H
Pt
Long range bonds (Weak)
Pt-decorated CNT

ACCEPTED MANUSCRIPT

DFT study of *β*-D-glucose adsorption on single-walled carbon nanotubes decorated with platinum. A bonding analysis

Alejandro J. González Fá[1,2], Valeria Orazi[1,3], Estela A. González[1,4], Alfredo Juan[1,4] and Ignacio López-Corral[2,5*]

[1] *Instituto de Física del Sur (IFISUR), UNS-CONICET, Av. Alem 1253, B8000 Bahía Blanca, Argentina.*

[2] *Departamento de Química, Universidad Nacional del Sur, Av. Alem 1253, B8000 Bahía Blanca, Argentina.*

[3] *Departamento de Ingeniería Eléctrica y de Computadoras, Universidad Nacional del Sur, Av. Alem 1253, B8000 Bahía Blanca, Argentina.*

[4] *Departamento de Física, Universidad Nacional del Sur, Av. Alem 1253, B8000 Bahía Blanca, Argentina.*

[5] *Instituto de Química del Sur (INQUISUR), UNS-CONICET, Av. Alem 1253, B8000 Bahía Blanca, Argentina.*

**Corresponding author. Fax: (+54) 291 4595142. E-mail address: ilopezcorral@uns.edu.ar (I. López-Corral).*

ACCEPTED MANUSCRIPT

Highlights

• All studied β-D-glucose/Pt/nanotube geometries show an energetically favorable adsorption process.

• The most favorable geometries were stabilized through van der Waals long-range interactions.

• Van der Waals forces modify the stability trend obtained with PBE in the studied geometries.

• The main bonding is through O atom from glucose to Pt-doped carbon nanotube.

• Overlap population and bonding order studies confirm the van der Waals influence in geometry stabilization.

ACCEPTED MANUSCRIPT

Abstract

Adsorption of *β*-D-glucose onto Pt decorated carbon nanotubes (CNTs) was studied using density functional theory (DFT) methods including van der Waals (vdW) forces. Several adsorption geometries were analyzed evaluating the aptitude of different atoms from*β*-D-glucose molecule to be bonded with a Pt atom previously supported. The influence of vdW interactions in structure stabilization was also studied using overlap population (OP) and bonding order (BO) analysis. The results show strong short-range bonds between the O atoms from *β*-D-glucose and Pt decoration. The long-range interactions, mainly from O and H atoms from the adsorbate, demonstrate a significant contribution for stabilization of some geometric configurations. In effect, adsorption geometries where glucose interacts though the O atom of the ring or –OH groups are favored by vdW forces, becoming the most stable systems. On the other hand, the geometry with the strongest O–Pt bond but a very small contribution from vdW interactions results less stable. DOS analysis shows the stabilization of *β*-D-glucose after adsorption and a strong chemical interaction with Pt/CNT.

Keywords: DFT, glucose, CNT, bonding.

Highlights

• All studied *β*-D-glucose/Pt/nanotube geometries show an energetically favorable adsorption process.

• The most favorable geometries were stabilized through van der Waals long-range interactions.

• Van der Waals forces modify the stability trend obtained with PBE in the studied geometries.

• The main bonding is through O atom from glucose to Pt-doped carbon nanotube.

• Overlap population and bonding order studies confirm the van der Waals influence in geometry stabilization.

ACCEPTED MANUSCRIPT

1. Introduction

Honey is a sweet food with high carbohydrate content produced by worker bees from the nectar and other substances present in the flowers. In all cases its composition varies depending on the species of plants visited by bees; however, their major components belong to glucose (Fig. 1) and fructose [1, 2]. Its high nutritional value, unique flavor and wide range of uses make honey a desirable food for consumers, and in turn, a product subject to various adulterations to lower its cost, in detriment of quality [3]. One of the main methods for the above-mentioned purpose is to add glucose syrup. This has become a topic of concern and subject of study in recent decades [4].

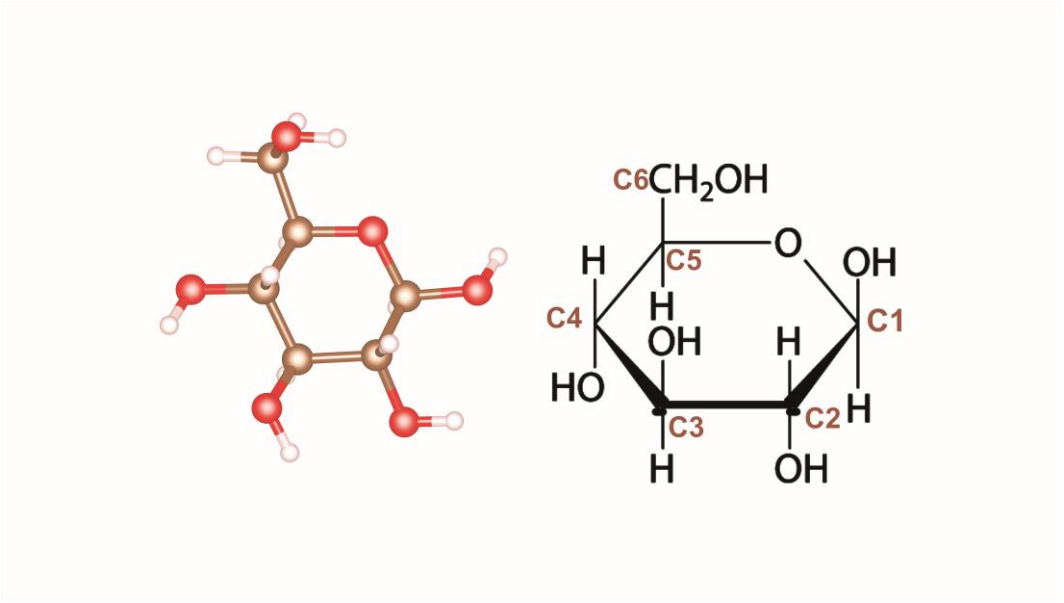

Figure 1. *β*-D-glucose molecule. The red, white and brown spheres correspond to oxygen, hydrogen and carbon atoms, respectively.

In order to avoid these problems, glucose monitoring has evolved over the last century with the development of more sensitive and sophisticated sensors. These can be classified into optical or electrochemical [5]. In the first group are those based on Forster resonance energy transfer (FRET) signals [6, 7] or derived from surface plasmon resonance (SPR) phenomenon[8, 9].On the other hand, electrochemical sensors can be classified into three generations. First generation was based on the entrapment of glucose oxidase enzyme (GO) in polymers or membranes linked to a mediator of electrons, which records signals produced by oxygen chemical reactions on the surface. Second generation includes new redox mediators replacing oxygen such as ferrocene, ferricyanide, quinines and thionine, among others. Third generation eliminates these mediators to reach higher selective and reagent less sensing. Finally, the last generation also uses nanomaterials (nanobiosensors), which dramatically increase the reproducibility, specificity and stability of these devices [5]. One

ACCEPTED MANUSCRIPT

example of biosensor is a graphene sheet interacting with chitosan, in glucose and cholesterol sensing [10]. Other interesting materials are carbon nanotubes (CNTs), which present excellent properties in heterogeneous catalysis because of their nanoscale size, high surface-to-volume ratio and chemical stability, allowing an excellent electrical communication between the surface and immobilized biocomponents that makes them ideal for high quality analytical biosensors [11,12]. The efficiency of these devices depends strongly on number of active sites capable of binding to the target analyte with high sensibility and reactivity [13]. The addition of transition metal atoms to CNTs (decorated CNTs) is a well-known strategy in glucose sensing technology [14, 15]. Other strategy is the functionalization of (5,5) boron nitride nanotubes, with hydroxyl and thiol groups [16]. Despite numerous experimental studies about this type of devices, there is a limited theoretical investigation about efficiency of these metals as active binding sites for adsorption of glucose on decorated CNTs. Ganji et al. [17] studied the glucose adsorption onto Pt-functionalized single-walled carbon nanotubes (SWCNTs), finding much higher interaction between the carbohydrate and the adsorbent than intrinsic nanotube without decoration.

In this work, we studied the properties of Pt-decorated SWCNTs as potential adsorbent of *β*-D-glucose by means of density functional methods, including van der Waals (vdW) interactions. We analyzed the influence of vdW forces on different adsorption geometries and focused on their role in the bonding mechanism and changes in the electronic structure.

2. Computational Method and Model

Spin-polarized DFT calculations were performed using the projector augmented wave (PAW) method [18] as implemented in the *Vienna Ab initio Simulation Package* (VASP) code [19-22]. We selected the generalized gradient approximation (GGA) exchange-correlation functional due to Perdew, Burke and Ernzerhof (PBE) [23, 24], with a cut-off energy of 520 eV for the plane-wave basis set expansion. The conjugate gradient algorithm was employed to relax the ionic positions, with a convergence criteria fixed at 10^{-3} eV/Å on each atom and 10^{-4} eV for the total energy. All atomic coordinates were allowed to relax during geometrical optimization. In order to ensure that we found indeed minimum energy structures, we checked the Hessian or performing a frequency analysis. After a first optimization, we utilize the final geometry as a new input with tighter energy gradient threshold and/or grid accuracy (by a factor of 10). The geometry converged to all-positive hessian eigenvalues within few cycles [25-27]. The effects of the vdW forces on the electronic and structure properties of the glucose/Pt/SWCNT system were evaluated by means of the vdW-DF functional [28-30]. These methods were successfully used in several

ACCEPTED MANUSCRIPT

opportunities in the simulation of different carbon structures and nanostructures [31-34].

We choose the typical (8,0) SWCNT. A one-dimensional periodic boundary condition was applied along the tube axis, with a supercell lattice constant of 8.53 Å (Fig. 2). The distance from the tube axis and its respective image was 20 Å in order to avoid any interaction between periodic images. The decoration of the (8,0) SWCNT was modeled adsorbing one Pt atom on a regular bridge site (above an axial C–C bond), which is the most preferable location of a single Pt atom on the carbon nanotube surface [35, 36]. In all calculations, a Monkhorst-Pack 1 × 7 × 1 k-point mesh [37] was taken for integration over the Brillouin zone (Fig. 2).

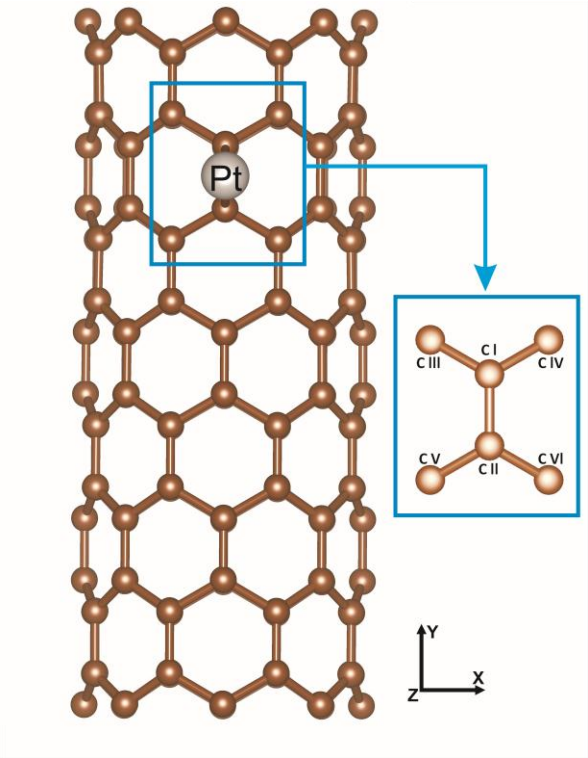

Figure 2. Pt-decorated carbon nanotube (seen from above).

Following a previous DFT study [17], four geometries were considered during the adsorption of *β*-D-glucose on the Pt-decorated (8,0) SWCNT. In those geometries the *β*-D-glucose molecule (Fig. 1) interacts with the Pt atom through different atoms: the O atom of the –COH group placed out of the ring (geometry 1); an O atom of an–OH group of the ring (geometry 2); the O atom of the ring (geometry 3); or an H atom of the ring (geometry 4). The different adsorption configurations are shown in Fig. 3. Other geometries presents less possibilities to develop long-range interactions .The adsorption energy (E_{ads}) of *β*-D-glucose on Pt-decorated SWCNT was defined as the difference between the total

ACCEPTED MANUSCRIPT

energy of glucose/Pt/SWCNT system and the sum of the energies of the isolated host (Pt-decorated SWCNT) and the isolated *β*-D-glucose molecule:

$$E_{ads} = E(\beta\text{-D-glucose/Pt/SWCNT}) - E(\text{Pt/SWCNT}) - E(\beta\text{-D-glucose}) \qquad (1)$$

According with this definition, a negative adsorption energy value corresponds to a stable interaction between the glucose molecule and the decorated nanotube.

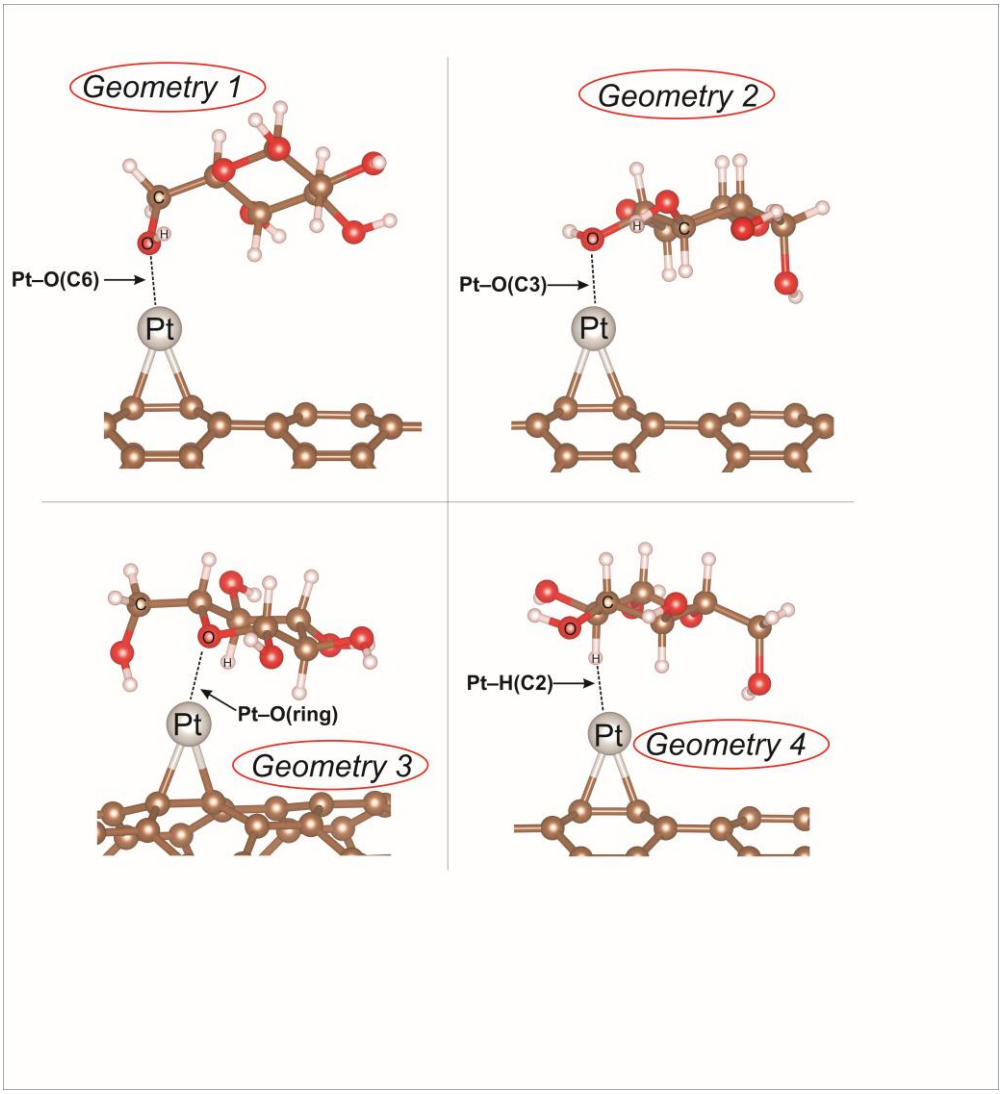

Figure 3. Studied geometries for *β*-D-glucose adsorption onto Pt/SWCNT and their main interactions (dotted lines). Glucose atoms were defined in Fig. 1.

We also performed a qualitative study of the bonding interactions developed during molecular adsorption of *β*-D-glucose. For this purpose, the bond order (BO) per atom and overlap population (OP) between atoms in extended structures [38,39] were computed for the previously optimized *β*-D-glucose/Pt/SWCNT geometries, using the DDEC6 method [40-42]. We also

ACCEPTED MANUSCRIPT

evaluated the atom-projected density of states (PDOS) in order to analyze the evolution of the electronic structure of glucose, Pt and SWCNT during the adsorption process. Finally, we computed the electronic charges on atoms using Bader analysis [43].

3. Results and Discussion

3.1. Geometrical optimization

We performed a full geometry optimization in order to obtain the most stable adsorption configurations. We found no magnetic moment for the Pt/SWCNT system, in concordance with results reported by Durgun et al. [32, 33]. Moreover, the projected magnetic moment for each Pt atom in *β*-D-glucose/Pt/SWCNT was found equal to zero in all cases.

Table 1 list the adsorption energy values corresponding to the different *β*-D-glucose/Pt/SWCNT configurations. Results from both PBE and vdW-DF calculations are included. It can be seen that in all cases negative values were obtained, which means that the adsorption is an energetically favorable process. Table 1 also shows that there are not significative differences among the PBE adsorption energies for geometries 1, 2 and 3 (see Fig. 3), being configuration 1 slightly favored. Geometry 4, in which the Pt decoration interacts with an H atom of the glucose ring, results unstable without dispersion forces.

Table 1. Adsorption energies for optimized *β*-D-glucose/Pt/SWCNT.

β-D-glucose/Pt/SWCNT system	E_{ads} (eV)	
	PBE method [23]	vdW-DF method [28-30]
Geometry 1	−1.07	−1.08
Geometry 2	−1.04	−1.15
Geometry 3	−1.03	−1.13
Geometry 4	—	−0.53

Table 1 also shows that total adsorption energy of configuration 1 does not change significantly by incorporating vdW interactions, but values that are slightly more negative are obtained in the case of geometries 2 and 3, thus modifying the trend achieved with the PBE functional. Geometry 4 results stable when vdW interactions are included, but presents the less negative adsorption energy. Consequently, it can be assumed that significant long-range interactions are developed between glucose and the decorated nanotube, providing stability to such systems. In a similar way, Ganji et al. [17] performed vdW-DF calculations with the SIESTA code and found more stable geometries

ACCEPTED MANUSCRIPT

when *α*-glucose is adsorbed on a Pt-decorated SWCNT through its O atoms, in particular through –OH and –COH groups.

3.2. Bonding analysis

We carried out a detailed OP and BO analysis on all optimized adsorption geometries, in order to describe the nature and evolution of chemical bonding. Table 2 shows the bond lengths and OP values corresponding to short-range interactions in isolated *β*-D-glucose, isolated Pt-decorated SWCNT and *β*-D-glucose/Pt/SWCNT systems. Comparison between PBE and vdW-DF results revealed only minor changes (up to 0.02 Å) in the bond lengths when dispersion forces are considered, except for C–Pt and Pt–O interactions, in which cases increments up to 0.03 Å and 0.06 Å, respectively, were found.

Table 2. Distances (*d*) and OP values, in parenthesis, for selected bonds in free *β*-D-glucose, isolated Pt/SWCNT and *β*-D-glucose/Pt/SWCNT systems.

Bond	Free *β*-D-glucose		Isolated Pt/SWCNT		*β*-D-glucose/Pt/SWCNT							
					Geometry 1		Geometry 2		Geometry 3		Geometry 4	
	d (Å)	OP	*d* (Å)	OP	*d* (Å)	OP	*d* (Å)	OP	*d* (Å)	OP	*d* (Å)	OP
Pt–O(C6)	—	—	—	—	2.18	0.44	—	—	—	—	—	—
Pt–O(C3)	—	—	—	—	—	—	2.22	0.39	—	—	—	—
Pt–O(ring)	—	—	—	—	—	—	—	—	2.23	0.36	—	—
Pt–H	—	—	—	—	—	—	—	—	—	—	1.98	0.22
C(I)–Pt	—	—	2.09	0.48	2.11	0.46	2.11	0.45	2.10	0.46	2.10	0.46
C(II)–Pt	—	—	2.09	0.48	2.09	0.48	2.10	0.47	2.11	0.46	2.11	0.45
C(I)–C(II)	—	—	1.47	0.65	1.45	0.68	1.45	0.68	1.45	0.68	1.46	0.67
O(C6)–H	0.97	0.54	—	—	0.98	0.50	0.98	0.54	0.99	0.55	0.98	0.54
O(C6)–C6	1.44	0.72	—	—	1.47	0.64	1.44	0.72	1.43	0.73	1.44	0.72
C5–O(ring)	1.46	0.64	—	—	1.46	0.64	1.46	0.64	1.50	0.58	1.46	0.63
C3–O(C3)	1.45	0.69	—	—	1.44	0.69	1.49	0.60	1.45	0.69	1.44	0.70
O(C3)–H	0.97	0.54	—	—	0.97	0.53	0.98	0.49	0.98	0.53	0.98	0.53
C1–O(C1)	1.42	0.72	—	—	1.41	0.72	1.41	0.72	1.40	0.74	1.41	0.72
O(C1)–H	0.97	0.54	—	—	0.97	0.53	0.97	0.53	0.98	0.52	0.97	0.53
C1–O(ring)	1.44	0.65	—	—	1.45	0.64	1.44	0.65	1.49	0.56	1.44	0.65

It can be seen in Table 2 that when *β*-D-glucose is adsorbed in geometry 1, a strong Pt–O interaction is developed between the Pt decoration and the O atom of the –COH group, with an OP value of 0.44 and a bond length of 2.18 Å. As a consequence, C–Pt bonds between the nanotube and the transition metal are lengthened up to 1.0 %, with a decrease of 2.6 % in the OP value. At the same time, the C–C bond from the bridge site in the SWCNT is contracted and strengthened 1.1 % and 3.6 %, respectively. In contrast, other C–C bonds of the

ACCEPTED MANUSCRIPT

decorated SWCNT are almost not affected. The adsorption process also causes changes in the atom–atom overlap populations of the *β*-D-glucose molecule, particularly in C6–O(Pt) and O(C6)–H bonds, which undergo a significant weakening (10.7 and 8.6% respectively). In the case of geometry 2, Table 2 shows that an important Pt–O bond is developed through the –OH group of the ring, with a length of 2.22 Å and an OP value of 0.39. As result of this adsorbate–substrate interaction, Pt–C(I) and Pt–C(II) bonds of the decorated SWCNT are elongated 1.3 % and 0.4 %, respectively, with a significant decrease in their OP values. Simultaneously, the C(I)–C(II) bond is strengthened 4.0 %, decreasing its distance 1.2 %. On the other hand, C3–O(Pt) and O(C3)–H bonds of *β*-D-glucose suffer a considerable weakening after adsorption, reducing their OPs in 12.9 % and 7.9 %, respectively.

For geometry 3, the interaction takes place mainly through O atom of the glucose's ring, reaching a Pt–O OP value of 0.36 and a bond distance of 2.23 Å. In this process, the bonds between Pt and C atoms from the nanotube are elongated approximately 1.0 %, with a decrease in OP up to 4.4 %. The C–C bond that supports the Pt-decoration is contracted 1.0 % and strengthened 3.4 %. At the same time, C–O5 and C–O1 bonds in *β*-D-glucose are noticeably weakened after adsorption. In fact, the populations of these bonds decrease 9.7 % (O–C5) and 13.2 % (O–C1), and their bond lengths are increased 2.5 % and 3.6 %, respectively. Finally, in geometry 4 the interaction is mainly through the H(C2), originating an H–Pt interaction with an OP value of 0.22 and a bond distance of 1.98 Å. Consequently, Pt–C(I) and Pt–C(II) bonds are elongated 0.8 % and 1.1%, respectively, while the corresponding OP values decrease up to 4.8 %. The C(I)–C(II) bond is also affected after adsorption: its OP value increases 0.6 % and its length decreases 2.1%.

Results from Table 2 shows that the Pt–O OP value is more important in geometry 1 than in the other configurations. However, more stable adsorption energy values are shown in Table 1 for geometries 2 and 3 when the vdW-DF method is included, so long-range interactions would also be taken into consideration. In this way, we analyzed total OP values belonging to selected interactions in the different glucose/adsorbent systems, with the objective to study the contributions of short and long-range bonding to the total Pt–O, Pt–C(glucose), Pt–H, C(SWCNT)–O or C(SWCNT)–H overlaps. Table 3 lists the OP sums obtained for the selected atom–atom interactions. It can be seen that for geometries 1 and 2 the short-range Pt–O overlaps (chemical bonds) contribute in 98.4 and 97.4 %, respectively, to the total Pt–O OP, while in geometry 3 this contribution decreases to 79.3%. This behavior suggests that geometry 3 present more long-range Pt–O interactions, which confers high stability to the adsorbed glucose. It can also be observed in Table 3 that long-range Pt–C(glucose), Pt–H, C(SWCNT)–O and C(SWCNT)–H overlaps are

ACCEPTED MANUSCRIPT

higher in geometry 2 and 3 than those belonging to geometry 1. In other words, short-range interactions between *β*-D-glucose and Pt/nanotube are the main interaction in geometry 1, while long-range interactions are more important in geometries 2 and 3. These long-range overlaps are less developed, but provide stability to the adsorbate, changing the stability order. Finally, the selected interactions showed in Table 3 for geometry 4 are in all cases similar to or smaller than those belonging to the other configurations, expect for the Pt–H overlap. Therefore, the less negative adsorption energy value was obtained for this geometry, as it can be seen in Table 1.

Table 3. OP sums belonging to selected short and long-range interactions for *β*-glucose/Pt/SWCNT systems.

Interaction	*β*-D-glucose/Pt/SWCNT			
	Geometry 1	Geometry 2	Geometry 3	Geometry 4
Pt–O	0.446	0.397	0.449	0.048
Pt–C(glucose)	0.042	0.081	0.124	0.047
Pt–H	0.081	0.125	0.190	0.281
C(SWCNT)–O	0.001	0.031	0.011	0.032
C(SWCNT)–H	—	0.021	0.041	0.011

The analysis of BO for those atoms that play an important role in the adsorption process shed more light into the bonding mechanism. Table 4 lists the sums of BO values (SBO) per relevant O, H and C atoms before and after the adsorption. The Pt SBO value corresponding to the Pt/SWCNT system without glucose is lower than that observed after adsorption, increasing for all the studied *β*-D-glucose/Pt/SWCNT geometries as a result of the new adsorbate–support interactions. Table 4 also shows that the SBO values belonging to C(I) and C(II), which support the decoration on the nanotube, undergo small changes after glucose interaction, for all the adsorption configurations, while C atoms away from the decoration point (C_{away}) almost do not show differences in their SBO values when glucose is adsorbed. Regarding O atoms, a different BO evolution is observed according to the adsorption configuration. In effect, Table 4shows that O(C6) increases its SBO value when geometry 1 is adopted. The major SBO increment for O(C3) corresponds to geometry 2, and per the O atom of the glucose's ring is observed for the geometry 3. In the case of H(C2), the most important SBO change takes place in the geometry 4, where a very important Pt–H(C2) interaction is developed.

ACCEPTED MANUSCRIPT

Table 4. SBO for the main atoms involved, before and after adsorption.

SBO	Free β-D-glucose	Isolated Pt/SWCNT	β-D-glucose/Pt/SWCNT			
			Geometry 1	Geometry 2	Geometry 3	Geometry 4
Pt	—	1.727	2.463	2.416	2.496	2.135
C(I)	—	4.082	4.100	4.101	4.104	4.087
C(II)	—	4.085	4.118	4.120	4.115	4.080
O(C6)	2.237	—	2.571	2.274	2.314	2.277
O(C3)	2.208	—	2.211	2.409	2.210	2.217
O(ring)	2.582	—	2.573	2.570	2.605	2.585
H(C2)	0.901	—	0.899	0.938	0.958	1.015
C_{away}	—	3.912	3.911	3.917	3.911	3.916

Finally, Table 5 details the contributions of different glucose's atoms to the total Pt BO values after adsorption. It can be seen for geometries 1, 2 and 3 that the O atoms present the most important contribution to the bonding with Pt. Geometry 3 shows the higher total contribution of the glucose's atoms to the total bonding with Pt atom: 0.895, which represents about 35.8% of the total Pt BO for this geometry. In the case of geometries2 and1, the contributions of glucose molecule to the total Pt BO are lower (31.0 and 30.5 %, respectively), in agreement with the smaller adsorption energy values computed for this geometry. Geometry 4 presents the lowest total contribution of the glucose's atoms to the total Pt BO, being only 23.6% of this BO value. Results from Table 5 suggests that in geometries 1, 2 and 3 the short and long-range Pt–H, Pt–C and Pt–H interactions are less strong than the Pt–O overlaps, but play a relevant contribution to the bonding mechanism. For geometry 4, the most important contribution in the adsorption process corresponds in the Pt–H interaction.

Table 5. Contributions of glucose atoms to the total Pt BO.

β-D-glucose atoms	BO Pt			
	Geometry 1	Geometry 2	Geometry 3	Geometry 4
O(C6)	0.617		0.043	0.009
O(C3)		0.523		0.028
O(ring)	0.002		0.465	0.021
other O atoms (sum)	0.005	0.011	0.055	0.019
H(C2)		0.041	0.040	0.256
other H atoms (sum)	0.084	0.089	0.164	0.064
C atoms (sum)	0.044	0.085	0.128	0.106
glucose's atoms (sum)	0.752	0.749	0.895	0.503
Total	2.463	2.416	2.496	2.135
% BO Pt-glucose	30.5	31.0	35.8	23.6

ACCEPTED MANUSCRIPT

3.3. Electronic structure

The electronic structure of the Pt/SWCNT and the glucose molecule are shown in Fig. 4. The total DOS shows stabilization after adsorption for the more stable geometries (see Fig. 4a and 4d). The total DOS of *β*-D-glucose/Pt/SWCNT shows a small shift to lower energies after adsorption. For geometry 3, the DOS curve is more extended in the energy range compared to geometry 2, being the last peaks located at –19.1 eV and –19.6 eV respectively. On the other hand, the total DOS in geometry 2 presents strong peaks in the energy region between –1.5 and –19.0 eV. The Pt atom and glucose PDOS after adsorption show also a shift to lower energies (see Fig. 4b to 4f). The PDOS for glucose-adsorbed molecule in geometry 2 show a sharp peak at –15.3 eV and a very small peak at –19.1 eV. In the case of geometry 3, the PDOS for glucose present the sharp peak at –12.0 eV and minor peaks at –15.4 eV and –19.6 eV. The different energy value for the sharp peaks in PDOS curves for glucose indicate that the geometry 2 is slightly more stable than geometry 3.

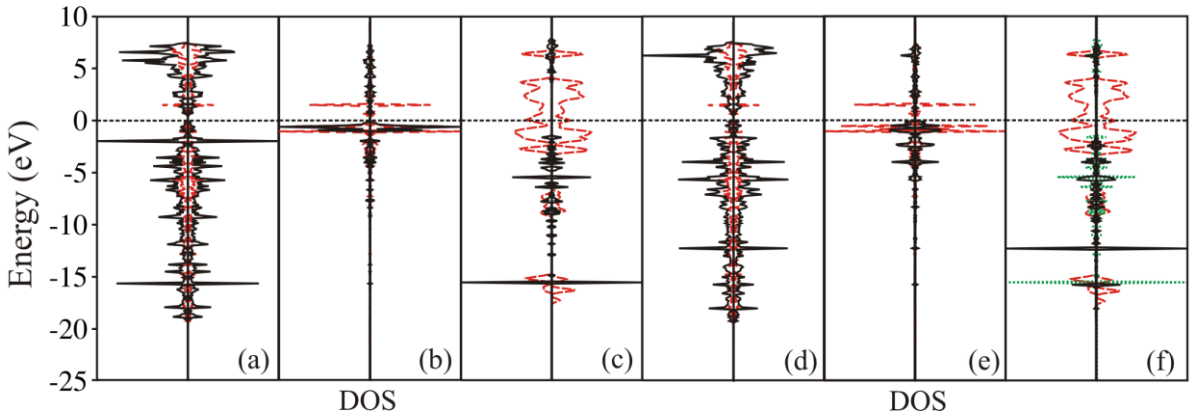

Figure 4. DOS plots curves for the *β*-D-glucose/Pt/SWCNT: (a) Total, (b) projected on Pt atom and (c) on glucose molecule for geometry 2; (d) Total, (e) projected on Pt atom and (f) on glucose molecule for geometry 3. The black fill line indicates system after glucose adsorption and the dashed red line correspond to Pt/SWCNT and glucose molecule at vacuum (before glucose adsorption). The green dotted line in (f) is the PDOS on glucose molecule for geometry 2.

The Pt–SWCNT interaction was affected by the adsorption as reveled by intensity peaks increment and shifts in energy. The sharp peaks at –5.5 and –15.3 eV for geometry 2 (at –5.6, –12.0 and –15.4 eV for geometry 3) coming from the glucose orbitals stabilized after adsorption (please compare Fig. 4a and 4c, and 4d and 4f). The peaks at (–2.1, –15.4) eV in Fig. 4b and at (–2.2, –15.5) eV in Fig. 4f correspond to the Pt–glucose interactions. The higher hybridization in the mentioned regions shows the glucose molecule orbitals

ACCEPTED MANUSCRIPT

interaction with the bottom of the *d* metal band and SWCNT (please compare Fig. 4a-4c and 4d-4f).

Finally, Fig. 5 shows the electron density distribution of glucose adsorbed in geometries 2 and 3. The charge density difference ($\Delta\rho$) isosurface was calculated using the following equation:

$$\Delta\rho = \rho(\beta\text{-D-glucose/Pt/SWCNT}) - \rho(\text{Pt/SWCNT}) - \rho(\beta\text{-D-glucose})$$

where ρ(Pt/SWCNT) is the charge density of the relaxed surface and ρ(*β*-D-glucose) is that one of the adsorbed molecule. In Fig. 5 it can be seen that the transferred charge between adsorbate and substrate is consistent with Bader difference charge (Table 6) and previous BO analysis. The main charge transfer seems to come from SWCNT to Pt and at the same time oxygen atoms O(C3) and O(ring) become more positive, so they are losing some electronic charge.

Table 6. Bader charges for selected atoms, before and after adsorption.

Bader charges	Free *β*-D-glucose	Isolated Pt/SWCNT	*β*-D-glucose/Pt/SWCNT	
			Geometry 2	Geometry 3
Pt	—	–0.050	–0.115	–0.243
C(I)	—	–0.031	0.088	0.018
O(C3)	0.449	—	1.596	1.734
O(ring)	0.261	—	1.519	1.425

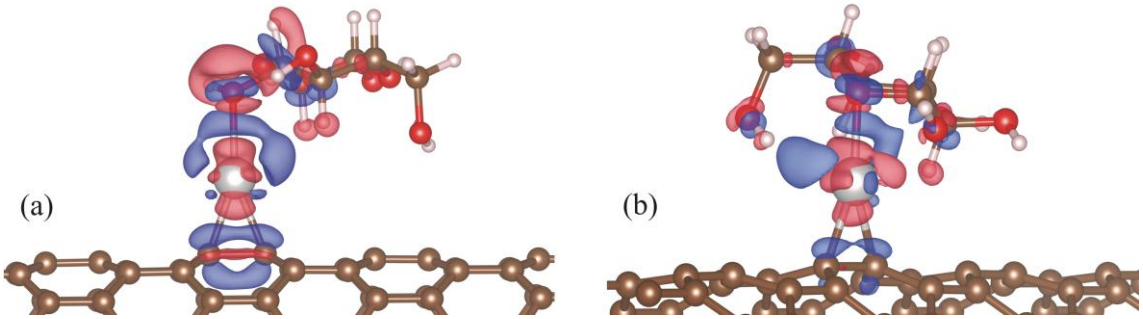

Figure 5. Charge distribution views around *β*-D-glucose adsorbed on Pt/SWCNT: (a) geometry 2 and (b) geometry 3. Red color indicates negative charge and blue positive charge.

4. Conclusions

The adsorption and stability of *β*-D-glucose onto Pt-decorated SWCNT were analyzed, in order to understand the main adsorbate–support interactions. We made special emphasis in the study of bonding properties through OP and BO

ACCEPTED MANUSCRIPT

analysis. Calculations without vdW forces shows a slight preference for geometry 1 with an adsorption energy of −1.07 eV, while geometries 2 and 3 were favored taking into account vdW interactions, with −1.15 eV and −1.13 eV respectively. Geometry 4 was not found stable without vdW forces. Pt−O was the main short-range bond found, particularly for structures 1, 2 and 3. However, OP values show an important contribution from long-range interaction for geometries 2 and 3 through *β*-D-glucose atoms away from the main union site, contributing in the stability for these structures. In this way, the O and H atoms located far from the Pt atom interact mainly with it, but also with C atoms from SWCNT. BO analysis confirms our OP study and the vdW influence in geometry stabilization cited before. Our results agree with those from previous works and provide an interesting OP, BO and DOS analysis that reveal the contribution of long-range interactions.

Acknowledgment

Our work was supported by PICT-ANPCyT 2014 (1351) and PIP-CONICET 2014-2016 (11220130100436CO), as well as by SGCyT-UNS. E. A. González, I. López-Corral and A. Juan are members of CONICET. A. J. González Fá and V. Orazi are fellows researcher at that Institution. The authors acknowledge useful discussion with Prof. M. S. Di Nezio.

References

[1] L. Wu, B. Du , Y. Vander Heyden , L. Chen, L. Zhao , M. Wang , X. Xue, Recent advancements in detecting sugar-based adulterants in honey – A challenge, Trends Analyt. Chem. 86 (2017) 25–38.

[2] S. Bogdanov, The honey book. Ed. Bee Product Science. 2014.Available in: http://www.bee-hexagon.net/Accessed. 23.11.12.

[3] P. Y. Qiu, H. B. Ding, Y. K. Tang, R. J. Xu,Determination of Chemical Composition of Commercial Honey by Near-Infrared Spectroscopy**,** J. Agric. Food. Chem. 47 (7)(1999)2760–2765.

[4] J. Wang, X. Xue, X. Du, N. Cheng, L. Chen, J. Zhao, J. Zheng, W. Cao, Identification of Acacia Honey Adulteration with Rape Honey Using Liquid Chromatography– Electrochemical Detection and Chemometrics, Food. Anal. Methods. 7(10) (2014) 2003–2012.

[5] V. Scognamiglio, Nanotechnology in glucose monitoring: Advances and challenges in the last 10 years, Biosens Bioelectron. 47 (2013) 12–25.

ACCEPTED MANUSCRIPT

[6] V. Scognamiglio, V. Aurilia, N. Cennamo, P. Ringhieri, L. Iozzino, M. Tartaglia, M. Staiano, G. Ruggiero, P. Orlando, T. Labella, L. Zeni, A. Vitale, S. D'Auria, D-galactose/D-glucose-binding Protein from Escherichia coli as Probe for a Non-consuming Glucose Implantable Fluorescence Biosensor, Sensors.7(10) (2007) 2484–2491.

[7] J.V. Veetil, S. Jin, K. Ye, A Glucose Sensor Protein for Continuous Glucose Monitoring, Biosens. Bioelectron. 26 (2010) 1650–1655.

[8]L. Tian, J. Qiu, Y. C. Zhou, S. G. Sun, Application of polypyrrole/GOx film to glucose biosensor based on electrochemical-surface plasmon resonance technique. Microchim. Acta.169 (2010) 269–275.

[9] A. Baba, P. Taranekar, R. R. Ponnapati, W. Knoll, R. C. Advincula, Electrochemical surface plasmon resonance and waveguide-enhanced glucose biosensing with N-alkylaminated polypyrrole/glucose oxidase multilayers, ACS Appl. Mater. Interfaces. 2 (2010) 2347–2354.

[10] E. Chigo Anota, A. Torres Soto, G. Cocoletzi, Studies of graphene–chitosan interactions and analysis of the bioadsorption of glucose and cholesterol, Appl. Nanosci. 8 (2014) 911–918.

[11] M. Musameh, J. Wang, A. Merkoci, Y. Lin, Low-potential stable NADH detection at carbon-nanotube-modified glassy carbon electrodes, Electrochem. Commun. 4 (10) (2002) 743–746.

[12]J. Li , H. T. Ng, A. Cassell, W. Fan, H. Chen , Q. Ye, J. Koehne , J. Han, M. Meyyappan, Carbon Nanotube Nanoelectrode Array for Ultrasensitive DNA Detection, Nano Lett. 3 (2003) 597–602.

[13] P. Pannopard,P. Khongpracha,M. Probst, J. Limtrakul, Gas sensing properties of platinum derivatives of single-walled carbon nanotubes: A DFT analysis, J. Mol. Graph. Model.28 (2009) 62–69.

[14]S. H. Lim, J. Wei , J. Lin,Q. Li, J. Kuayou , A glucose biosensor based on electrodeposition of palladium nanoparticles and glucose oxidase onto Nafion-solubilized carbon nanotube electrode, Biosens. Bioelectron. 20 (11) (2005) 2341–2346.

[15] Z. Wen, S. Ci, J. Li, Pt Nanoparticles Inserting in Carbon Nanotube Arrays: Nanocomposites for Glucose Biosensors, J. Phys. Chem. C. 113 (31) (2009) 13482–13487.

[16] E. Chigo Anota, G. Cocoletzi, First-principles simulations of the chemical functionalization of (5,5) boron nitride nanotubes, J. Mol. Model. 19 (2013) 2335-2341.

ACCEPTED MANUSCRIPT

[17] M. D. Ganji, F. S. E. Skardi, Adsorption of Glucose Molecule onto Platinum-Decorated Single-Walled Carbon Nanotubes: A Dispersion-Corrected DFT Simulation, Fuller. Nanotub. Carb. N. 23:3 (2015) 273–282.

[18] P. E. Blochl, Projector Augmented-wave Method, Phys. Rev. B: Condens. Matter. Mater. Phys. 50 (1994) 17953−17979.

[19] W. Kohn, L. J. Sham, Self-Consistent Equations Including Exchange and Correlation Effects, Phys. Rev. A: At., Mol., Opt. Phys. 140 (1965) 1133−1138.

[20] G. Kresse, D. Joubert, From Ultrasoft Pseudopotentials to the Projector Augmented Wave Method, Phys. Rev. B: Condens. Matter Mater. Phys. 59 (1999) 1758−1775.

[21] G. Kresse, J. Furthmüller, Efficiency of Ab-initio Total Energy Calculations for Metals and Semiconductors Using a Plane-wave Basis Set, Comput. Mater. Sci. 6 (1996) 15−50.

[22] G. Kresse, J. Furthmüller, Efficient Iterative Schemes for Ab Initio Total-energy Calculations Using a Plane-wave Basis Set, Phys. Rev. B: Condens. Matter. Mater. Phys. 54 (1996) 11169−11186.

[23] J. P. Perdew, K. Burke, M. Ernzerhof, Generalized Gradient Approximation Made Simple, Phys. Rev. Lett. 77 (1996) 3865−3868.

[24] J. P. Perdew, K. Burke, M. Ernzerhof, M. Erratum: Generalized Gradient Approximation Made Simple, Phys. Rev. Lett. 78 (1997) 1396−1396.

[25] A. P. Rahalkar, V. Ganesh, S. R. Gadre, Enabling ab initio Hessian and frequency calculations of large molecules, J. Chem. Phys. 129 (2008) 234101−234107.

[26] A. F. Izmaylov, G. E. Scuseria, Efficient evaluation of analytic vibrational frequencies in Hartree-Fock and density functional theory for periodic nonconducting systems, J. Chem. Phys. 127 (2007) 144106−144114.

[27] T. Buèkoa, J. Hafner, J. G. Ángyán, Geometry optimization of periodic systems using internal coordinates, J. Chem. Phys. 122 (2005) 124508−124517.

[28] M. Dion, H. Rydberg, E. Schröder, D.C. Langreth, B.I. Lundqvist, Van der Waals density functional for general geometries, Phys. Rev. Lett. 92 (2004) 246401−246404.

[29] G. Román-Pérez, J.M. Soler, Efficient implementation of a van der Waals density functional: application to double-wall carbon nanotubes, Phys. Rev. Lett. 103 (2009) 096102−096105.

ACCEPTED MANUSCRIPT

[30]J. Klimes, D.R. Bowler, A. Michelides,Chemical accuracy for the van der Waals density functional,J. Phys.: Cond. Matt. 22 (2010)022201−022205.

[31] J. Kleis, E. Schröder, P. Hyldgaard, Nature and strength of bonding in a crystal of semiconducting nanotubes: van der Waals density functional calculations and analytical results, Phys. Rev. B. 77 (2008) 205422−205431.

[32] L. Gao, Y. Liu, R. Shi, T. Ma, Y. Hu, J.Luo, Influence of interface interaction on the moiré superstructures of graphene on transition-metal substrates, RSC Adv. 7 (2017) 12179–12184.

[33] I. López-Corral, S. Piriz, R. Faccio, A. Juan, M. Avena, A van der Waals DFT study of PtH_2 systems absorbed on pristine and defective graphene, Appl. Surf. Sci. 382 (2016) 80–87.

[34] P. Lazic, Z. Crljen, Graphyne on metallic surfaces: A density functional theory study, Phys. Rev. B. 91 (2015) 125423−125427.

[35] E. Durgun, S. Dag , V. M. K. Bagci, O. Gülseren, T. Yildirim, S. Ciraci, Systematic study of adsorption of single atoms on a carbon nanotube, Phys. Rev. B. 67 (2003) 201401−201404.

[36] E. Durgun, S. Dag, S. Ciraci, O. Gülseren. Energetics and electronic structures of individual atoms adsorbed on carbon nanotubes, J. Phys. Chem. B. 108 (2004) 575−582.

[37] H. J. Monkhorst, J. D. Pack, Special Points for Brillouin-zone Integrations, Phys. Rev. B: Solid State. 13 (1976) 5188−5192.

[38] R.J. Hoffmann, Solids and Surfaces: A Chemist's View of Bonding in Extended Structures, VCH, New York, 1988.

[39] R. Dronskowski, Computational Chemistry of Solid State Materials: A Guide for Materials Scientists, Chemists, Physicists and others, Wiley-VCH, Weinheim, 2005.

[40] T. A. Manz and N. Gabaldon-Limas, Introducing DDEC6 atomic population analysis: part 1.Charge partitioning theory and methodology, RSC Adv. 6 (2016) 47771−47801.

[41] N. Gabaldon-Limas, T. A. Manz, Introducing DDEC6 atomic population analysis: part 2. Computed results for a wide range of periodic and non periodic materials, RSC Adv. 6(2016) 45727−45747.

ACCEPTED MANUSCRIPT

[42] T. A. Manz, N. Gabaldon Limas, Chargemol program for performing DDEC analysis, Version 3.4.4, 2016, ddec.sourceforge.net.

[43] R.F.W. Bader, Atoms in Molecules - A Quantum Theory, Oxford University Press, Oxford, 1990.